62. C. Chothia and J. P. Pauling, *Nature* **219**, 1156 (1968).
63. We also fitted the organophosphoryl moiety of monoisopropylphosphoryl-chymotrypsin in a way analogous to that observed in the crystal structure of this conjugate of Cht (M. Harel *et al.*, *J. Mol. Biol.*, in press) with an organophosphate that is also a powerful AChE inhibitor. Determining the structure of similar organophosphate conjugates of AChE itself would help improve our current model of ACh binding and help us map the topography of the active site.
64. J. E. Purdie and R. A. McIvor, *Biochim. Biophys. Acta* **128**, 590 (1966); R. D. O'Brien, *Biochem. J.* **113**, 713 (1969); J. C. Meunier and J. P. Changeux, *FEBS Lett.* **2**, 224 (1969).
65. M. I. Kabachnick *et al.*, *Pharmacol. Rev.* **22**, 355 (1970).
66. G. M. Steinberg, M. L. Mednick, J. Maddox, R. Rice, J. Cramer, *J. Med. Chem.* **18**, 1056 (1975).
67. H. A. Berman and M. M. Decker, *J. Biol. Chem.* **264**, 3951 (1989); H. A. Berman and K. Leonard, *ibid.*, p. 3942.
68. G. Amitai and P. Taylor, in *Cholinesterases: Structure, Function, Mechanism, Genetics and Cell Biology*, J. Massoulie *et al.*, Eds. (American Chemical Society, Washington, DC, 1991), p. 285.
69. H.-J. Nolte, T. L. Rosenberry, E. Neumann, *Biochemistry* **19**, 3705 (1980).
70. J. A. Tainer, E. D. Getzoff, J. S. Richardson, D. C. Richardson, *Nature* **306**, 284 (1983); E. D. Getzoff *et al.*, *ibid.*, p. 287.
71. D. R. Davies and H. Metzger, *Annu. Rev. Immunol.* **1**, 87 (1983).
72. M. Dennis *et al.*, *Biochemistry* **27**, 2346 (1988); J. L. Galzi *et al.*, *J. Biol. Chem.* **265**, 10430 (1990).
73. G. Adam and M. Delbruck, in *Structural Chemistry and Molecular Biology*, A. Rich and N. Davidson, Eds. (Freeman, San Francisco, 1968), pp. 198–215; M. Eigen, in *Quantum Statistical Mechanics in the Natural Sciences*, S. L. Mintz and S. M. Widmayer, Eds. (Plenum, New York, 1974), pp. 37–61.
74. T. L. Rosenberry and E. Neumann, *Biochemistry* **16**, 3870 (1977).
75. A. J. Howard *et al.*, *J. Appl. Crystallogr.* **20**, 383 (1987).
76. W. Kabsch, *ibid.* **21**, 916 (1988).
77. R. E. Dickerson, J. E. Weinzierl, R. A. Palmer, *Acta Crystallogr.* **B24**, 997 (1968).
78. Abbreviations for the amino acid residues are: A, Ala; C, Cys; D, Asp; E, Glu; F, Phe; G, Gly; H, His; I, Ile; K, Lys; L, Leu; M, Met; N, Asn; P, Pro; Q, Gln; R, Arg; S, Ser; T, Thr; V, Val; W, Trp; and Y, Tyr.
79. J. P. Priestle, *J. Appl. Crystallogr.* **21**, 572 (1988).
80. M. Harel, C. T. Su, F. Frolow, I. Silman, J. L. Sussman, *Biochemistry* **30**, 5217 (1991).
81. We thank M. Lachever for help in various stages of this research, O. Herzberg, A. Wlodawer, J. Remington, J. Massoulié, W. Peticolas, B. P. Doctor, D. Ollis, and F. Winkler for valuable discussions, and M. Levitt for his stimulating comments and help in preparing Fig. 7B using the MacIMDAD program. We are also grateful to S. Nidam for his expert photography, O. Bahar for her skilled graphics work, and C. Palustran for help in preparing the manuscript. Supported by U.S. Army Medical Research and Development Command contract no. DAMD17-89-C-9063, the Minerva Foundation, the Revson Foundation, Association Franco-Israélienne pour la Recherche Scientifique et Technologique, the United States–Israel Binational Science Foundation (BSF), Jerusalem, and the Kimmelman Center for Biomolecular Structure and Assembly, Rehovot. I.S. is Bernstein-Mason Professor of Neurochemistry. A.G. is a Markey fellow, and his work on this project was supported by the Lucille P. Markey Charitable Trust. This paper is dedicated to Irwin B. Wilson.

18 April 1991; accepted 12 July 1991

Impact-Induced Cleaving and Melting of Alkali-Halide Nanocrystals

RAINER D. BECK, PAMELA ST. JOHN, MARGIE L. HOMER, ROBERT L. WHETTEN

Impact of nanocrystalline alkali-halide clusters against solid surfaces causes them to fission exclusively into low surface-energy fragments. In time-of-flight scattering experiments, this process appears at an impact energy so low that it must result from a single-step cleavage of the nanocrystal along low surface-energy cleavage planes. At higher energies (more than 1 electron volt per atom), a crossover occurs to an entirely different behavior—evaporative cascades that proceed irrespective of the structure-energetic properties of the fragments. These cascades, and the approximately linear scaling of the crossover energy with cluster size, are characteristic of impact-induced transformation of the cluster to a molten state. Collision with the high-rigidity surface of silicon gives a substantially greater cleavage probability than the soft basal-plane surface of graphite.

IMPACT OF SOLID PROJECTILES AGAINST SOLID SURFACES IS associated with a range of important phenomena (*1*). Sticking or adhesion leads to aggregation and growth of overlayers or the condensed phase. At higher energies, implantation of material into the solid becomes feasible. Ricochet processes include shattering or melting of the scattered projectile. The relative significance of these processes depends upon the effectiveness of the interactions, within and between the projectile and target materials, in accommodating the impact momentum. Investigation of the impact phenomenon of the smallest solids, namely atomic or compound clusters, could allow one to obtain a microscopic understanding of empirical laws governing these phenomena.

Despite a number of reports on scattering of uncharged molecular clusters at hyperthermal energy (*2*) and of mass-selected clusters at much higher energies, (*3*) there has been no well-defined collision experiment, in which the mass and structure of an incident solid cluster are known along with the collision energy and nature of the surface. Of particular interest is the range bounded below by hyperthermal speeds and above by the strongest chemical interactions (approximately 0.05 to 5 eV per atom), where short-range repulsive interactions are dominant (*4*) and implantation or sputtering are unfeasible. Advances in cluster-beam methods (*5*) make it possible to use internally cold, mass-selected cluster beams injected into a scattering chamber under well-defined angular, velocity, and surface conditions. We report studies of collisions of the smallest crystalline objects, specifically the alkali-halide clusters (AHCs), with soft and hard surfaces—highly oriented graphite (0001) and silicon (100)—under conditions fulfilling these criteria.

Cluster formation and acceleration. Ionic compound clusters, including the alkali-halide clusters (AHCs), have the rock-salt ionic bonding of the bulk crystal (*6–12*), that is, they are nanocrystals. Structures of the most stable clusters have cuboid morphology, as shown in Fig. 1, that can be derived from the bulk crystal by cleaving it along mutually perpendicular planes so that only (100) faces are exposed. Less stable clusters are obtained by forming terraces on a

---

The authors are in the Department of Chemistry, University of California, Los Angeles, CA 90024.

face of a smaller cuboid (*6, 9*). Charged clusters of the form $M_nX_{n-1}^+$ and $M_{n-1}X_n^-$ are readily produced (*8, 9*) and have appropriate electron-binding energies (*10*) to minimize surface electron-transfer processes (neutralization). Completely filled, charged cuboids arrange the $2n - 1$ ions in a lattice having (j,k,l) ions on the edges and are possible whenever $2n - 1 = j \times k \times l$ (all odd) (*12*). The smallest of these, a (3,3,3) cube, is a particle just smaller than one cubic nanometer, given typical interatomic spacings (0.25 nm). The two inert surfaces used here—highly oriented graphite (0001) and passivated single-crystal silicon (100)—are chemically inert toward alkali-halide compounds and have high work functions (ϕ = 5 eV and 4.6 eV, respectively).

In the cluster-surface collider (Fig. 2), cluster projectiles formed in a laser-ablation source (*8*) are entrained in and cooled by a helium nozzle-jet expansion to yield an intense, pulsed beam. Charged clusters are mass-selected so that only a selected cluster size *n* enters the collision chamber. This packet is retarded to the desired momentum and angle of impact; the scattered, charged particles are accelerated in the same field toward the detector. The graphite surface [highly oriented pyrolytic graphite (HOPG)] is cleaned by heating for several hours at 450°C (*13*), which removes the hydrocarbon overlayer, as verified by observing the intensity of ions sputtered from the adsorbate. The silicon surface is heated similarly, but no attempt is made to remove the oxide passivation layer. In operation, the beam energy and surface angle are selected to collect a certain fraction of scattered fragments. Because a substantial fraction of the parallel momentum is lost or exchanged during the collision, the surface angle must be set away from the specular angle in order to collect uniformly both the intact scattered cluster and its fragments. Charged fragments are mass-analyzed through their flight time in the secondary flight region because the instrument operating voltage greatly exceeds the collision energy. The uncertainty in time of collision is typically $10^{-8}\,n^{1/2}$ s (the peak width in the field-reflected ions). The root-mean-square collision energy spread is typically no greater than σ_E = 5 eV.

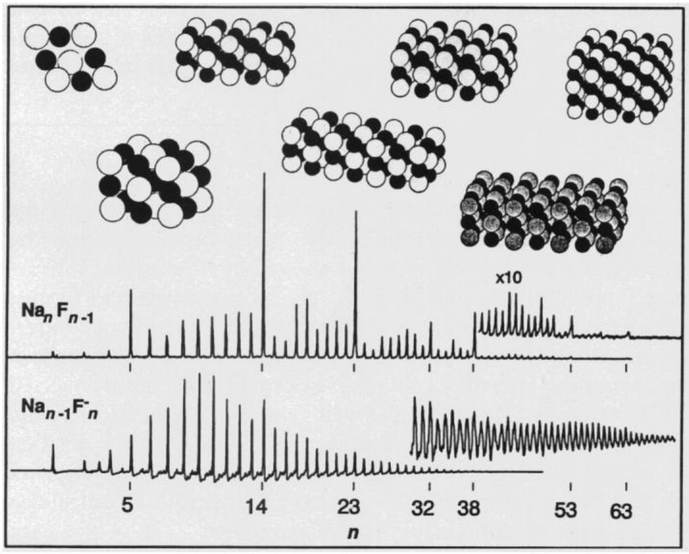

Fig. 1. (**Top**) Relaxed structures of cuboid nanocrystalline alkali-halide clusters, $Na_nF_{n-1}^+$. [From left to right: lattice dimension (j,k,l) given in parentheses: n = 5 (1,3,3), n = 14 (3,3,3), 23 (3,3,5), 32 (3,3,7), 38 (3,5,5), 53 (3,5,7), and 63 (5,5,5).] (**Bottom**) Relative abundances of the positively and negatively charged clusters, as measured by reflectron mass spectrometry. The upper spectrum selected is for intentionally heated clusters, in order to expose the magic numbers. The colder clusters used for scattering have abundances with only minor ledges.

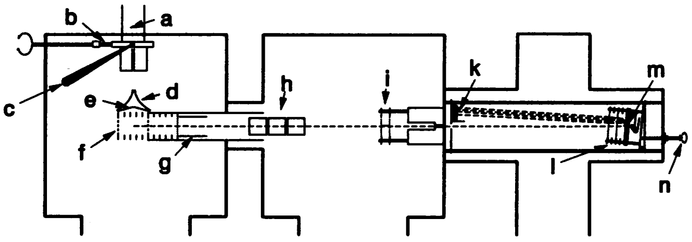

Fig. 2. Scale diagram of the cluster-beam collider apparatus, consisting of three chambers. The source chamber (left) contains the pulsed valve (a) releasing a 0.01 SF_6/He mixture at 10-bar pressure, the alkali-coated rod and drive shaft (b) inserted into the nozzle block, which contains a perpendicular channel for the ablation-laser beam (c); the gas jet is skimmed by the mechanical skimmer (d), with the resulting beam shape determined by slits (e), prior to entering the pulsed extraction field region (f). The trajectory of the extracted ions (horizontal dashed lines; typically 2-keV beam energy) passes into the second chamber (middle, base pressure < 10^{-7} torr), where it is steered by the horizontal deflection plates (g), focused in the far field by the einzel lens (h), and mass-filtered by the temporal mass gate (*29*) (i), which consists of a thin, charged wire on the beam axis whose voltage is zeroed during the time-window when the desired cluster-mass packet passes. The scattering chamber (at right, base pressure < 10^{-9} torr) contains the retarding field screens (l) (1 to 2 keV over 1 to 2 cm), the scattering surface (m) (heated radiatively from behind), and a mechanical drive (n) to set the angle with respect to the fixed detector (10° with respect to the incident beam) at (k).

Fragmentation spectra. We have investigated a number of (M,X) combinations, with the $Na_nF_{n-1}^+$ series (n = 2 to 43) explored in greatest detail, in collisions with graphite and silicon over an energy range from nominal zero up to 200 eV (Fig. 3). At lowest energies (nominal zero), the major observed process is prompt inelastic scattering of the intact cluster. At higher energies, sufficiently large clusters (n > 13) exhibit two distinct collision regimes with a crossover energy that scales with the size of the cluster, *n*. Charged-fragment mass spectra (Figs. 3 and 4) show that low energy impact (0.2 to 1.0 eV per atom) yields very specific fragments, while at high energy (1 to 5 eV per atom) a broad distribution of fragments of the recoiled cluster is observed. Smaller clusters, n < 14, do not have these clear-cut regimes, but instead always fragment in a manner reminiscent of molecular ions (*14*) in accordance with noncrystalline structures (*6*).

The specific fragmentation channel can be interpreted as a cleaving of the incident nanocrystal. For example, collisions with graphite or silicon below 40 eV impact energy split the n = 23 clusters exclusively into the n = 14 (Figs. 3 and 4). This is obtained by cleaving the (3,3,5) cuboid nanocrystal parallel to a (100) face to give a charged n = 14 (3,3,3) and uncharged n = 9 (2,3,3) (Fig. 5). This channel is even more dominant in $K_{23}F_{22}^+$, and when the harder Si surface is used as a target (Fig. 3D)—the elastic constant of Si ($K = 0.99 \times 10^{11}$ N m^{-2}) is twice that of NaF (0.48×10^{11}) and is eight times the component perpendicular to the layered basal plane of graphite ($C = 0.12 \times 10^{11}$) (*15*). When the incident cluster is not a cuboid, the cleavage of the outer terrace occurs at even lower energies and completely dominates the distribution, as seen in Fig. 3, C and D. Generally, these clusters show one or more cleavage pathways as the exclusive fragmentation channels at lowest impact energies; for example, impact of n = 24 to 27 yields m = 23 and 14, and n = 34 yields both m = 32 and 23.

Consideration of the computed energies required by various fragmentation channels shows that this process could not result from a sequence of NaF losses, an evaporative cascade:

$$Na_nF_{n-1}{}^+ \rightarrow Na_mF_{m-1}{}^+ + (n - m)\,\mathrm{NaF}\;\; E_b(n,m) \quad (1)$$

even assuming the entire collision energy is imparted to the internal modes of the scattered cluster. Computed energies $E_b(n,m)$ of the fragments from process 1, an example of which is shown in Fig. 4B, are directly relevant because the attractive interactions between the inert (or passivated) surface and the cluster is small compared to the ionic bonding energies. As an example, to produce the $n = 14$ cuboid from the $n = 23$ cuboid through a sequence of NaF emissions requires more than 20 eV, yet it is clearly observed at $E_i < 20$ eV (graphite) and at nominal zero (silicon). However, consideration of the single-step fracture processes of the type

$$\mathrm{Na}_n\mathrm{F}_{n-1}{}^+ \rightarrow \mathrm{Na}_m\mathrm{F}_{m-1}{}^+ + (\mathrm{NaF})_{n-m} \quad E_f(n,m) \qquad (2)$$

shows that the energy $E_f(23,14)$ to cleave $n = 23$ to $m = 14$ and $n - m = 9$ is 3.3 eV (Fig. 4B), and can account for the exclusiveness of this product at lowest energies. [The cleavage energy can also be estimated from the surface area created (twice the cross-sectional area of the $n = 14$ cluster or ~1 nm^2) and the bulk surface energy (200 erg/cm^2), which yields an energy of 2.5 eV to cleave along a face. Computed energies do not include three-body polarization effects (*6*), which favor placing the charge on the larger cleavage fragment at the expense of otherwise competitive channels like $\mathrm{Na_5F_4}^+ + (\mathrm{NaF})_{18}$.]

The observed influence of surface characteristics—in particular, the greater extent and selectivity of cleavage from impact with rigid Si over soft graphite—suggests that the dominance of the cleavage process is specific to excitation by impact, occurring on the collision timescale ($\tau < 10^{-12}$ s). However, the only rigorous bound on this quantity comes from our time-of-flight measurement, $\tau << 5 \times 10^{-8}$ s, from the peak width in Fig. 3D. Total energy calculations, for a complete range of n, indicate that cleavage generally is the easiest fragmentation channel, but the energetic preference is not large and statistical considerations clearly favor evaporation (*16*).

In the high-energy regime, the fragment patterns of all of the larger clusters are dominated by a smooth, statistical-like distribution. In remarkable contrast to the low E_i abundance patterns, these distributions show little or no enhancement at the stable clusters $n = 14$ and 23 (*17*). In fact, the trend in Fig. 4 indicates that these are parallel, or competing, processes, since the initial yield of $n = 14$ decreases to the benefit of larger fragments $n = 15$ to 21. The tendency of the mean size of the charged fragment to decrease monotonically with energy is consistent with the dominance of process (*2*), stepwise evaporation, as had already been seen in metastable decay of sputtered CsI clusters (*18*). [Some of this fragmentation is not prompt (on the 10^{-7}-s time scale), as seen by the asymmetric broadening of the mass peaks at threshold.] A statistical model (*19*) of the fragmentation process is then appropriate, in which one uses the evaporation energies $E_b(n,m)$, for estimating the distribution of internal energies U imparted to the incident cluster during the collision. As a typical example, Fig. 5 shows how the distribution's mean, U, varies with collision energy for the case of the $n = 23$ cluster. In the nearly linear region of the plot, approximately 35 percent of the impact energy goes toward cluster heating (*20*), consistent with previous reports that collisions of molecular ions with solid surfaces deposits a large, relatively well-defined energy into the ion (*14*).

Analysis of the peak flight times also demonstrates that the collisions are highly inelastic events. By fitting the fragment time-of-flight peaks to a common time-to-mass scale, one finds that the events leading to fragmentation are properly described as prompt scattering (no trapping desorption) in which most or all of the incident perpendicular momentum is lost. [A significant spread in this quantity is observed, as the scattering peaks are significantly broader than the unscattered (reflectron) peaks.] Furthermore, the peak for the intact parent clusters shows both a prompt component and a broader delayed component (doublets in Fig. 3). At increased collision energy, the delayed component is diminished relative to the prompt component, integrated over mass, and shifts to longer delay time. A reasonable interpretation is that the incident cluster either scatters promptly—and, depending on energy, subsequently fragments or is detected intact—or it is trapped, dissipating the impact energy into the surface and desorbing intact at later times, resulting in the observed broad line shape. At high collision energies, the nonfragmenting events are rare and occur exclusively through surface trapping—ultimately enabling nearly all of the impact energy to be dissipated—followed by desorption. As indicated above, angular measurements show that a substantial portion of the parallel momentum is also lost or exchanged, although this momentum may not be very important in heating the cluster (*21*).

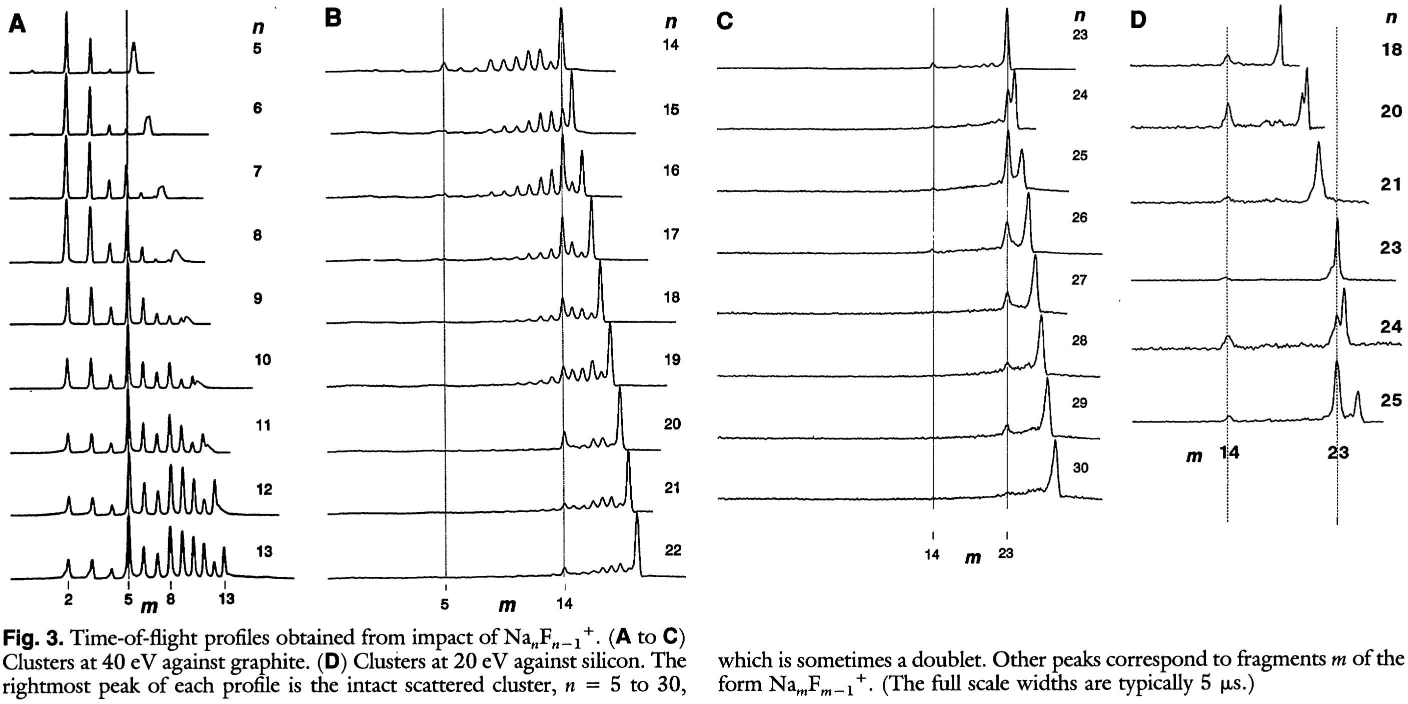

Fig. 3. Time-of-flight profiles obtained from impact of $\mathrm{Na}_n\mathrm{F}_{n-1}{}^+$. (**A** to **C**) Clusters at 40 eV against graphite. (**D**) Clusters at 20 eV against silicon. The rightmost peak of each profile is the intact scattered cluster, $n = 5$ to 30, which is sometimes a doublet. Other peaks correspond to fragments m of the form $\mathrm{Na}_m\mathrm{F}_{m-1}{}^+$. (The full scale widths are typically 5 μs.)

Nanocrystal-surface interactions. Gathering these separate perspectives into a single picture, it is seen that prompt cluster-surface scattering events are highly inelastic, with nearly all the incident kinetic energy dissipated in the internal heating of the cluster (up to 35 percent) and in the surface (the remaining 65 percent or more). The impact-deposited energy induces cleavage or evaporative decay, with a crossover to the latter occurring at an impact energy near $E_i = 1$ eV per atom, corresponding to an internal heating at crossover U_c near 0.35 eV per atom. We now give an interpretation of this quantity as the energy required to transform the incident cluster to its molten form. Assuming bulk quantities, the energy required to heat (from $T = 0$ K) and completely melt a Na_nF_{n-1} crystal is given approximately at sufficiently large n by

$$\Delta E = 6nk_B T_m + n\Delta H_f \qquad (3)$$

where the two terms represent the heat of fusion $\Delta H_f = 0.30$ eV per molecule and energy to heat the solid oscillators to the melting temperature, $T_m = 1266$ K, so that $6k_B T_m = 0.65$ eV per molecule. The energy to melt is therefore $\Delta E/2n = 0.47$ eV per atom. This is larger than $U = 0.35$ eV per atom estimated above. A depressed T_m [owing to finite-size effect (*7*)], combined with incident cluster temperatures above absolute zero, should make up the difference.

Accordingly, at low energies the fragmentation corresponds to the fracture of the suddenly heated or stressed solid, which takes account of the incident cluster's structure and easy cleavage planes. At high energies the fragmentation pattern is the featureless one of a liquid, which ignores the existence of crystalline structures. That the crossover energy, at which the fluid first dominates over the solid behavior, appears to scale with size is a manifestation of the approximate extensivity of the heat capacity.

Essentially identical fragmentation patterns have been obtained on negatively charged sodium-fluoride clusters containing the same total number of ions (Fig. 1), indicating that the role of Na^+ and F^- ions in the nanocrystal lattice can be reversed without changing the results. Impact of the $K_nF_{n-1}{}^+$ clusters against graphite results in a similar crossover from cleavage to evaporation with equal or better distinction. However, experiments on lithium-fluoride clusters to $n = 30$ failed to show the two distinct processes; in the absence of detailed simulations, we suggest that small LiF clusters may not assume rigidly crystalline structures. In contrast to the alkali-halides, other systems examined show no evidence for cleavage: impact of molecular clusters $(H_2O)_nH^+$ and network clusters $C_n{}^+$ ($n = 60$, 84) collide to yield smooth fragment distributions and no fragmentation, respectively. Prior investigations of cluster fragmentation—energized by photons, by gas-phase collisions, by the ionization event, or by their own heat of formation—found dominant mechanisms including stepwise monomer or dimer evaporation from molecular (*22*) and metal (*5*) clusters and AHCs (*18*), emission of favored "molecular" fragments from network-forming clusters (C_n, Si_n) (*23*), and fissioning of transition metal clusters specific to the parent cluster (*24*). In contrast, we find that impact-induced fragmentation of sufficiently large ionic clusters occurs in an intrinsically macroscopic manner by fracturing along

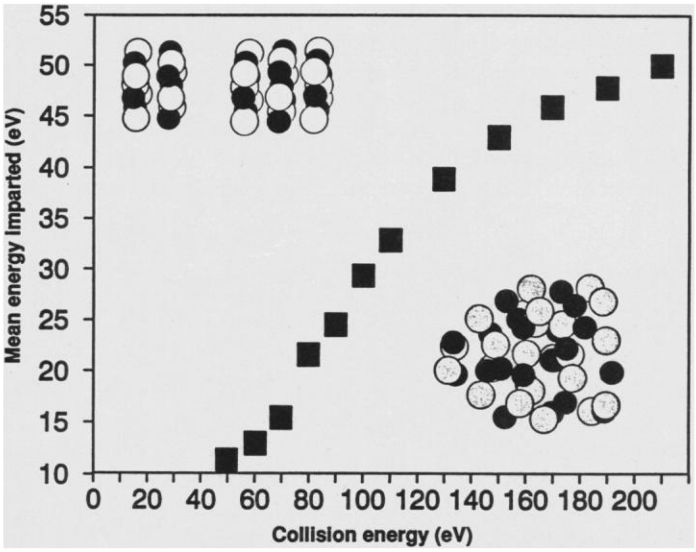

Fig. 5. The mean energy U imparted to the $Na_{23}F_{22}{}^+$ by impact against graphite at energy E_i, as calculated by a simple statistical model (*19*). An essentially identical result is obtained with Si, over the indicated energy range. Structures illustrate the low-energy cleavage channel (above left) and the molten cluster at 1000 K (lower right).

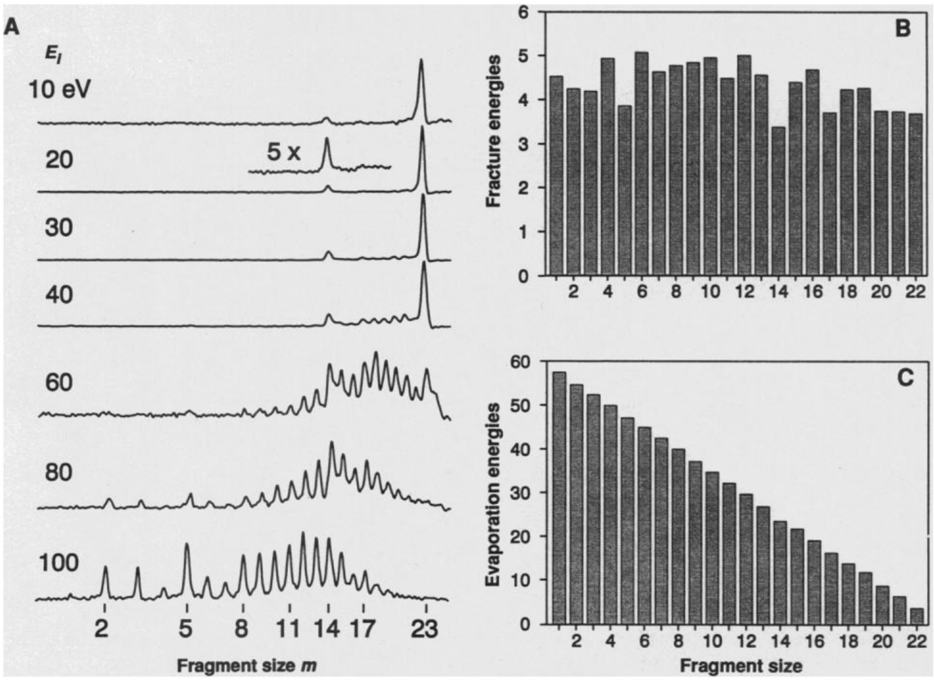

Fig. 4. (**A**) Time-of-flight profiles resulting from impact of $Na_{23}F_{22}{}^+$ (3,3,5) against Si at the indicated energies. The $m = 14$, 13 fragment is produced by a "cleaving" process even at the lowest collision energy. The computed energies $E_f(23,m)$ and $E_b(23,m)$ required to yield observed fragments by (**B**) a single fracture (process 2), or (**C**) by an evaporative cascade 1 from an $Na_{23}F_{22}{}^+$ cluster. Quantities are computed by methods described in (*6*) and (*16*) in which standard empirical potentials neglecting polarization were used (three-body terms).

the cleavage planes of the incident crystal.

Our results are in accord with the macroscopic cleavage process, insofar as it is modeled by ideal crystals: Only (100) planes show simple cleavage, but the measured cleavage energy is orders of magnitude smaller than predicted by microscopic theory (*25*). Nanoscopic crystals can be selected by mass so as to be free of the spurious stresses present in real macroscopic crystals; imperfect clusters might be suitable for approximating the effect of these stresses. More generally, microscopic simulations of impact-induced cleaving and melting processes and the energy accommodation should be of interest as new impact phenomena (*26*). Collision between an atomic or compound cluster and a solid surface constitutes a crucial step in the so-called soft-landing method of forming new cluster-assembled materials through ionized or neutral cluster-beam deposition (*27*). Trapping-desorption phenomena observed here deserve careful attention with regard to the soft-landing hypothesis. Harder collisions are primarily of interest in the formation of high-quality thin films (*27*). Properties of deposited clusters and their fragments should be probed, as a function of impact energy, with surface analytical tools. Exploration of other nanocrystal-surface processes by these methods are possible, including chemical reaction with the surface and electron-transfer.

Note added in proof: Recent work (*29*) on the photofragmentation of alkali bromides and iodides shows that electronic excitation leads exclusively to neutral halogen emission, further establishing the interpretation of the impact-induced clearing. We have also found a new low-energy channel in the impact of larger sodium-fluoride clusters against silicon—loss of F^- to yield $Na_nF_{n-2}{}^{2+}$—interpreted as a direct chemical reaction with the surface (*30*).

REFERENCES AND NOTES

1. W. Goldsmith, *Impact* (Arnold, London, 1960).
2. See R. J. Holland, G. Q. Xu, J. Levkoff, A. Robertson, S. L. Bernasek, *J. Chem. Phys.* **88**, 7952 (1988); A. A. Vostrikov, D. Yu. Dubov, M. R. Predtechenskii, *Sov. Phys. Tech. Phys.* **33**, 1153 (1989); U. Even, P. J. deLange, H. T. Jonkman, J. Kommadeur, *Phys. Rev. Lett.* **56**, 965 (1986).
3. R. J. Beuhler, G. Friedlander, L. Friedman, *Phys. Rev. Lett.* **63**, 1292 (1989); *Science* **245**, 1448 (1989). For review, see R. J. Beuhler and L. Friedman, *Chem. Rev.* **86**, 521 (1986).
4. For a recent comprehensive review of molecule-surface hyperthermal collision processes, see A. Amirav, *Comments At. Mol. Phys.*, in press.
5. L.-S. Zheng, P. J. Brucat, C. L. Pettiette, S. Yang, R. E. Smalley, *J. Chem. Phys.* **83**, 4273 (1985).
6. T. P. Martin, *Phys. Rep.* **95**, 167 (1983). See also E. C. Honea, thesis, University of California, Los Angeles (1990).
7. J. Luo, U. Landman, J. Jortner, in *Physics and Chemistry of Small Clusters*, P. Jena, B. K. Rao, S. N. Khanna, Eds. (Plenum, New York, 1987), pp. 201–206; J. Luo, thesis, Georgia Institute of Technology, Atlanta (1988).
8. E. C. Honea, M. L. Homer, R. L. Whetten, *Int. J. Mass Spectrom. Ion Processes* **102**, 213 (1990).
9. C. W. S. Conover, Y. A. Yang, L. A. Bloomfield, *Phys. Rev.* **B38**, 3517 (1988).
10. E. C. Honea, M. L. Homer, P. Labastie, R. L. Whetten, *Phys. Rev. Lett.* **63**, 394 (1989); G. Rajagopal *et al.*, *ibid.* **64**, 2933 (1990).
11. P. J. Ziemann and A. W. Castleman, *J. Chem. Phys.*, in press; T. P. Martin and T. Bergmann, *ibid.* **90**, 6664 (1989).
12. J. E. Campana *et al.*, *ibid.* **47**, 1046 (1981).
13. J. Suzanne, J. P. Coulomb, M. Bienfait, *Surf. Sci.* **44**, 141 (1974).
14. For review of the surface-induced dissociation method applied to molecular ions, see R. G. Cooks, T. Ast, Md. A. Mabud, *Int. J. Mass Spectrom. Ion Processes* **100**, 209 (1990).
15. R. Nicklow, N. Wakabayashi, H. G. Smith, *Phys. Rev.* **B5**, 4951 (1972); J. M. Soler, A. M. Baro, N. García, H. Rohrer, *Phys. Rev. Lett.* **57**, 444 (1986); G. Simmons and H. Wang, *Single Crystal Elastic Constants and Calculated Aggregate Properties* (MIT Press, Cambridge, MA, ed. 2, 1971).
16. M. L. Homer, in *Alkali Halide Vapors*, P. Davidovits and D. L. McFadden, Eds. (Academic Press, New York, 1979).
17. For example, see W. Ens, R. Beavis, K. G. Standing, *Phys. Rev. Lett.* **50**, 27 (1983). The disappearance of abundance anomalies (magic numbers) occurs when exceptionally hot clusters are measured at shortest times. The clusters are so hot as to remain fluids: J. Gspann, *Z. Phys.* **D3**, 143 (1986).
18. H-J. Hwang, D. K. Sensharma, M. A. El-Sayed, *Chem. Phys. Lett.* **160**, 243 (1989); *Phys. Rev. Lett.* **64**, 808 (1990).
19. H. I. Kenttämaa and R. G. Cooks, *Int. J. Mass Spectrom. Ion Processes* **64**, 79 (1985).
20. Removing the surface coverage (hydrocarbon overlayer) and elevated surface temperature (to 350°C) increased the extent of fragmentation slightly. Examples shown were recorded at ambient temperature with the hydrocarbon layer present.
21. For comments on parallel momentum, see J. C. Tully, *J. Chem. Phys.* **92**, 680 (1990).
22. M. L. Alexander, M. A. Johnson, N. E. Levinger, W. C. Lineberger, *Phys. Rev. Lett.* **57**, 976 (1986).
23. For review, see J. C. Phillips, *Chem. Rev.* **86**, 619 (1986).
24. S. K. Loh, L. Lian, D. A. Hales, P. B. Armentrout, *J. Chem. Phys.* **89**, 3378 (1990).
25. F. Seitz, *The Modern Theory of Solid* (McGraw-Hill, New York, 1940), pp. 96–98.
26. U. Landman, private communication.
27. For example, P. Fayet *et al.*, *Phys. Rev. Lett.* **55**, 3002 (1985); see also R. P. Andres *et al.*, *J. Mater. Res.* **4**, 704 (1989), and references therein.
28. R. D. Beck and R. L. Whetten, in preparation.
29. X. Li, R. D. Beck, R. L. Whetten, in preparation.
30. P. St. John, R. D. Beck, R. L. Whetten, unpublished.
31. This research was funded by the Office of Naval Research. The authors thank E. C. Honea and M. M. Alvarez for early technical advice and assistance, and R. S. Williams for providing the surface samples. Crucial discussions of surface scattering with R. S. Williams, D. Baugh, and the late R. B. Bernstein are also acknowledged. M.L.H. and R.L.W. acknowledge support from a University of California Dissertation Year Fellowship and a Packard Foundation Fellowship, respectively.

22 March 1991; accepted 1 July 1991